Jin *et al. Chin. J. Mech. Eng.* (2019) 32:64
https://doi.org/10.1186/s10033-019-0376-0

Chinese Journal of Mechanical Engineering

ORIGINAL ARTICLE

Open Access

Study on Rollover Index and Stability for a Triaxle Bus

Zhilin Jin[1*], Jingxuan Li[1], Yanjun Huang[2] and Amir Khajepour[2]

Abstract

Vehicle rollover, and its resulting fatalities, is an actively researched topic especially for multi-axle vehicles in the field of vehicle dynamics and control. This paper first presents a new rollover index for a triaxle bus to accurately evaluate its rollover possibility and then discusses the influence laws of the vehicle rollover dynamics to explore the mechanism of its stability. First, a six degree of freedom rollover model of the triaxle bus is developed, including lateral, yaw, roll motion of the sprung mass of the front/rear axle, and roll motion of the unsprung mass of the front/rear axle. Next, some key parameters of the vehicle rollover model are identified. A new rollover index is deduced according to the basics of vehicle dynamics, to predict vehicle rollover risk for the triaxle bus, which is verified by TruckSim. Furthermore, the influence laws of vehicle rollover dynamics by vehicle parameters and road parameters are discussed based on the simulation results. More importantly, the results show that the new method of modeling can precisely describe the rollover dynamics of the studied bus, and the proposed new index can effectively evaluate the rollover possibility. Therefore, this study provides a theoretical basis to improve anti-rollover ability for triaxle buses.

Keywords: Rollover stability, Dynamic model, Triaxle bus, Rollover index, Vehicle active safety

1 Introduction

Vehicle rollover is a serious safety accident. Among more than 6 million police-reported motor vehicle crashes that occurred in the United States in 2014, only 2.0% involved vehicle rollovers, with the proportion of rollover accidents leading to fatal crashes being 18.9% [1]. Some heavy vehicles are more likely to rollover due to their high center of gravity (CG), large mass and so on. Therefore, it is important for heavy vehicles to improve their active safety [2]. Triaxle buses, with a high center of gravity and long wheelbase, are often reported in rollover accidents with many passengers lost. As a result, accurately evaluating the possibility and exploring the mechanism of dynamic stability of a triaxle bus is important.

Over the years, it is necessary to establish an accurate and effective rollover dynamic model to predict vehicle roll motion. As a basic vehicle model, the two degrees of freedom (DOF) vehicle model with four wheels was used, which considered the road bank angles by Yu et al. [3, 4]. Also, the rollover dynamics state can be more accurately expressed by adding the roll plane model. So, a three-DOF model with lateral, yaw and roll motion is used by Zhang et al. [5]. Furthermore, the vertical motions of sprung and unsprung masses are added to the three-degree-of-freedom model by Jin et al. [6]. Considering the effect of the road excitation, a seven-DOF combined model was proposed based on a vehicle with a traditional chassis by Bao et al. [7]. In addition, a nonlinear eight-DOF model was put forward including longitudinal, lateral, yaw, roll, and four-wheel rotational motions [8, 9]. In order to reflect the vehicle dynamic characteristics in different directions, a dynamic model with sixteen-DOF was presented, including longitudinal, lateral, yaw, vertical, pitch, roll motions of the vehicle body; the rotational motion of four wheels, and vertical motions of the unsprung masses [10]. Na et al. proposed a new four-node membrane element model based on bending modification [11]. The verification and validation procedures are presented for the originally developed FE model of a Para transit bus, which was built by Bojanowski [12].

*Correspondence: jinzhilin@nuaa.edu.cn
[1] Department of Vehicle Engineering, Nanjing University of Aeronautics & Astronautics, Nanjing, Jiangsu Province 210016, China
Full list of author information is available at the end of the article

Although numerous research studies have been done on vehicle rollover, few have focused on triaxle buses. Wei Liu et al. [13] presented an integrated chassis stability control for the triaxle electric bus. In order to analyze the roll dynamics, an effective rollover index is indispensable. In recent years, many effective rollover indexes have been proposed. Vehicle speed is a key factor to prevent rollover, a safety speed model for rollover prevention is built under the condition of vehicle rapid rotation [14]. Lateral-load transfer ratio (LTR) is one of the most commonly used rollover indexes. To make the traditional LTR more accurate, the effect by uncertainties in the height of the vehicle's center of gravity, road disturbances, and possible multiple sensor faults are considered based on a nonlinear two-wheel vehicular system [15]. Phanomchoeng et al. [16] developed a new rollover index using the lateral acceleration as well as the vertical acceleration to detect both tripped and untripped rollovers. For heavy articulated vehicles with multiple axles, Huang et al. [2] proposed a multiple-rollover-indices. Li et al. [17] introduced an improved predictive LTR (IPLTR) which was based on an 8-DOF nonlinear vehicle model. Furthermore, as a dominant factor in vehicle rollover accident, drivers' operations should also be considered. An extended model of a driver-vehicle closed-loop system, with the time delay of driver's operation was proposed by Jin et al. [18]. Li et al. [19] analyzed the vehicle lateral stability and anti-rollover, which considered the effect of road excitation. A rollover coefficient is defined by Odenthal et al. that basically depends on the lateral acceleration to activate the emergency steering and braking system [20]. Imine et al. [21] proposed an estimator to estimate the vehicle rollover stability, including roll angle, yaw rate, and lateral acceleration.

In addition, some actuation systems have been presented, such as active steering, differential braking, active suspension, active anti-roll bar, and integrated chassis control. Gaspar et al. [22] studied the brake systems to obtain the anti-roll moment to realize anti-rollover of heavy vehicles. The combination of steering and braking control is applied to avoid rollover by Odenthal et al. [20]. Vu et al. [23] used active anti-roll bar as an actuator to improve the roll stability of heavy vehicles. A novel control method of Invariance Control is applied by Wollherr et al. [24].

In this paper, taking a tour bus 3A as research object, a method of modeling a triaxle bus rollover dynamic is developed and, taking the deflection of the flexible frame into consideration, a new evaluation method of rollover is proposed to detect the possibility of the triaxle bus rollover. Also, the dynamic rollover stability of the triaxle bus is analyzed.

This paper is organized as follows: in Section 2, the dynamic model of triaxle bus rollover is established, including yaw, lateral, and roll motion. Then, the real axles of the triaxle bus are considered equivalent to a virtual rear axle to simplify the dynamics. Section 3 proposes a new rollover index is proposed to detect the rollover risk and it is also verified in two different cases. In addition, the roll dynamics stability of the triaxle bus is simulated in typical maneuvers, and the influence laws of rollover stability of vehicle parameters and driving factors are discussed in Section 4. Furthermore, the roll stability of anti-external disturbances is analyzed in Section 5. Finally, some conclusions are made in Section 6.

2 Roll Dynamic Model of the Triaxle Bus

2.1 Triaxle Bus Model

Given the exclusive features of a triaxle bus, such as the high center of gravity, the long wheelbase, the large number of passengers' capacity, and the variable distribution of passengers having an impact on its roll property; the triaxle bus is divided into the front and the rear part. For a triaxle bus, the middle and rear axle are on the same side of the center of mass, and the distance between them is short such that the roll coupling can be neglected. Therefore, the middle and rear axle of the triaxle bus is equivalent to a virtual rear axle, as shown in Figure 1.

The distance between the first axle and the virtual rear axle is the equivalent wheelbase, which will be obtained in Section 2.3. In addition, a twisted bar with a constant stiffness is assumed to link between the front axle and the virtual rear axle.

For the sake of simplicity, the influence of the pitching, the lateral wind, and longitudinal motion are neglected, the road profile is regarded as symmetric with respect to the x axle. Thus, a six-DOF vehicle model is established, as shown in Figure 2.

From D'Alembert's principle, the motions of the above model are as follows.

Lateral motion:

$$ma_{\mathrm{y}} - m_{\mathrm{sf}}h_{\mathrm{f}}\ddot{\varphi}_{\mathrm{sf}} - m_{\mathrm{sr}}h_{\mathrm{r}}\ddot{\varphi}_{\mathrm{sr}} = 2F_{\mathrm{Y1}}\cos\delta + 2F_{\mathrm{Yr}}. \tag{1}$$

Yaw motion:

$$I_Z\dot{r} = 2aF_{\mathrm{Y1}}\cos\delta + M_{\mathrm{r}}. \tag{2}$$

Roll motion of the front sprung mass of the front axle:

$$\begin{aligned} I_{\mathrm{Xf}}\ddot{\varphi}_{\mathrm{sf}} = {} & m_{\mathrm{sf}}h_{\mathrm{f}}a_{\mathrm{y}} + m_{\mathrm{sf}}gh_{\mathrm{f}}\varphi_{\mathrm{sf}} - k_{\mathrm{f}}(\varphi_{\mathrm{sf}} - \varphi_{\mathrm{uf}}) \\ & - l_{\mathrm{f}}(\dot{\varphi}_{\mathrm{sf}} - \dot{\varphi}_{\mathrm{uf}}) + k_{\mathrm{b}}(\varphi_{\mathrm{sf}} - \varphi_{\mathrm{sr}}). \end{aligned} \tag{3}$$

Roll motion of the sprung mass of the rear axle:

$$\begin{aligned} I_{\mathrm{Xr}}\ddot{\varphi}_{\mathrm{sr}} = {} & m_{\mathrm{sr}}h_{\mathrm{r}}a_{\mathrm{y}} + m_{\mathrm{sr}}gh_{\mathrm{r}}\varphi_{\mathrm{sr}} - k_{\mathrm{r}}(\varphi_{\mathrm{sr}} - \varphi_{\mathrm{ur}}) \\ & - l_{\mathrm{r}}(\dot{\varphi}_{\mathrm{sr}} - \dot{\varphi}_{\mathrm{ur}}) + k_{\mathrm{b}}(\varphi_{\mathrm{sr}} - \varphi_{\mathrm{sf}}). \end{aligned} \tag{4}$$

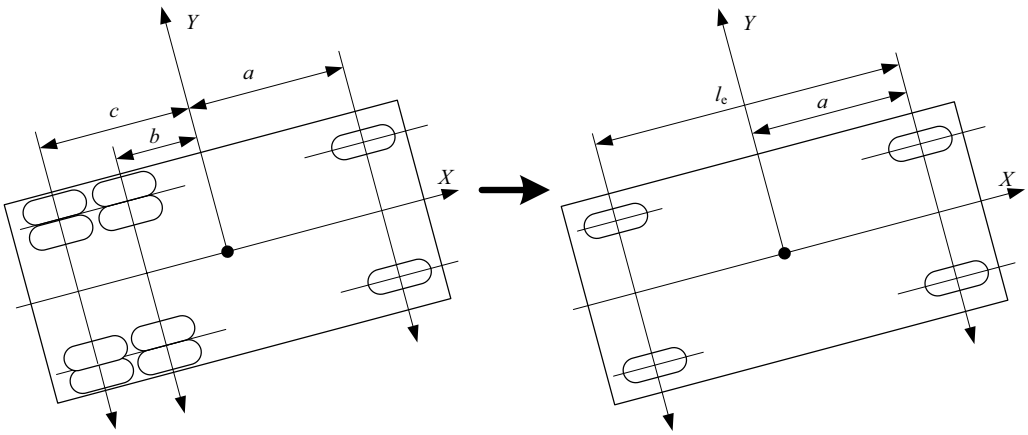

Figure 1 The equivalent model of the triaxle bus

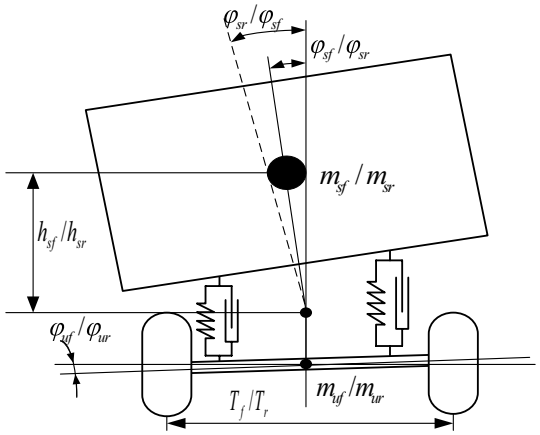

Figure 2 Dynamic model of the triaxle bus rollover

Roll motion of the unsprung mass of the front axle:

$$2F_{Y1}h_c + m_{uf}(h_{uf} - h_{cf})a_y = -m_{uf}g(h_{uf} - h_{cf})\varphi_{uf} - k_f(\varphi_{sf} - \varphi_{uf}) - l_f(\dot{\varphi}_{sf} - \dot{\varphi}_{uf}) + k_{uf}\varphi_{uf}. \tag{5}$$

Roll motion of the unsprung mass of the virtual rear axle:

$$2(F_{Y2} + F_{Y3})h_c + m_{ur}(h_{ur} - h_{cr})a_y = k_{ur}\varphi_{ur} - m_{ur}g(h_{ur} - h_{cr})\varphi_{ur} - k_r(\varphi_{sr} - \varphi_{ur}) - l_r(\dot{\varphi}_{sr} - \dot{\varphi}_{ur}), \tag{6}$$

where the lateral acceleration of the sprung mass is:

$$a_y = \dot{v} + ur, \tag{7}$$

and

$$\begin{cases} F_{Yr} = F_{Y2} + F_{Y3}, \\ M_r = 2bF_{Y2} + 2cF_{Y3}. \end{cases} \tag{8}$$

In above-mentioned equations, m denotes the total mass of triaxle bus. m_s shows the total sprung mass. m_f means the unsprung of mass vehicle. m_{sf} and m_{sr} represent the equivalent sprung mass of the front and the rear axle. m_{uf} and m_{ur} refer to the unsprung mass of the front and the rear axle. a, b and c are the longitudinal distance from the CG to the front axle, middle axle and rear axle, respectively. a_y is the lateral acceleration. u is the longitudinal speed, and v denotes the lateral velocity. r denotes the yaw rate of the sprung mass. h_f is the height between the center of front sprung mass and the roll center, while h_r is the height between the center of rear sprung mass and the roll center. h_{uf} and h_{ur} are the height of the center of the front unsprung mass and the rear unsprung mass, measured upwards from the road. h_{cf} and h_{cr} are the height of the front roll center and the rear roll center, measured upwards from the road, respectively. I_{Xf} and I_{Xr} are the roll inertia of the front sprung mass and the rear sprung mass, measured about the roll axle. I_z is yaw inertia of the triaxle bus. φ_{sf} and φ_{sr} are the roll angle of the front sprung mass and the rear sprung mass. F_{Yr} the lateral force of the tires at the virtual axle, M_r is the yaw moment caused by the virtual rear axle. F_{Y1}, F_{Y2} and F_{Y3} are the lateral force of the tires at the first axle, the middle axle and the rear axle, respectively. k_f and k_r are the equivalent roll stiffness coefficient of the front suspension and the rear suspension. k_{uf} and k_{ur} are the equivalent roll stiffness coefficient of the front unsprung mass and the rear unsprung mass. l_f and l_r are the equivalent roll damping coefficient of the front suspension and the rear suspension. k_b is the torsion stiffness coefficient of vehicle frame.

In addition, the steering angle of front wheels δ is assumed to be sufficiently small that $\cos\delta \approx 1$ in Eqs. (1) and (2) holds.

The lateral forces in Eqs. (1) and (2) mainly depending on the physical properties of the tire and the corresponding side slip angles β_f, β_m and β_r observed on the front, middle and rear wheels. The slip angle can be determined from the simple geometric relations:

$$\begin{cases} \beta_f = \arctan\left(\dfrac{v+ar}{u}\right) - \delta_f, \\ \beta_m = \arctan\left(\dfrac{v-br}{u}\right), \\ \beta_r = \arctan\left(\dfrac{v-cr}{u}\right). \end{cases} \tag{9}$$

Simplify the tire model with the cornering stiffness of tires is constant, the lateral forces of tires can be obtained.

$$\begin{cases} F_{Y1} = -K_f\beta_f, \\ F_{Y2} = -K_m\beta_m, \\ F_{Y3} = -K_r\beta_r, \end{cases} \tag{10}$$

where K_f, K_m and K_r are the cornering stiffness of the front wheels, the middle wheels and the rear wheels.

$$M_3 = \begin{bmatrix} h_f m_{sf} & 0 \\ h_r m_{sr} & 0 \\ -m_{uf}(h_{uf}-h_{cf}) & 0 \\ -m_{ur}(h_{ur}-h_{cr}) & 0 \end{bmatrix}, \quad M_4 = \begin{bmatrix} 0 & 0 & 0 & 0 \\ 0 & 0 & 0 & 0 \\ 0 & 0 & l_f & 0 \\ 0 & 0 & 0 & l_r \end{bmatrix},$$

$$M_5 = \begin{bmatrix} -I_{Xf} & 0 \\ 0 & -I_{Xr} \\ 0 & 0 \end{bmatrix}, \quad M_6 = \begin{bmatrix} 1 & 0 & 0 & 0 \\ 0 & 1 & 0 & 0 \end{bmatrix},$$

$$A_1 = \begin{bmatrix} \frac{-(2K_f+2K_m+2K_r)}{u} & \frac{-(mu^2+2aK_f-2bK_m-2cK_r)}{u} \\ \frac{-(2aK_f-2bK_m-2cK_r)}{u} & \frac{-(2a^2K_f+2b^2K_m+2c^2K_r)}{u} \end{bmatrix},$$

$$A_2 = \begin{bmatrix} 0 & -h_f m_s u \\ 0 & -h_r m_{sr} u \\ \frac{-2K_f h_c}{u} & \frac{m_{uf}u^2(h_{uf}-h_{cf})-2aK_f h_{cf}}{u} \\ \frac{-2(K_m+K_r)h_c}{u} & \frac{m_{ur}u^2(h_{ur}-h_{cr})+2bK_m h_{cr}+2cK_r h_{cr}}{u} \end{bmatrix},$$

$$A_3 = \begin{bmatrix} k_b + k_f - m_{sf}gh_f & -k_b & -k_f & 0 \\ -k_b & k_b + k_r - m_{sr}gh_r & 0 & -k_r \\ k_f & 0 & -k_{uf} + m_{uf}g(h_{uf}-h_{cf}) - k_f & 0 \\ 0 & k_r & 0 & -k_{ur} + m_{ur}g(h_{ur}-h_{cr}) - k_r \end{bmatrix}$$

2.2 State Space Model of System

Setting $U = \begin{bmatrix} \varphi_{sf} & \varphi_{sr} & \varphi_{uf} & \varphi_{ur} \end{bmatrix}^T$, $V = \begin{bmatrix} \dot{\varphi}_{sf} & \dot{\varphi}_{sr} \end{bmatrix}^T$ and substituting Eqs. (9) and (10) into Eqs. (1)–(8), the following equation of state space can be obtained:

$$M_q \begin{bmatrix} \dot{v} \\ \dot{r} \\ \dot{U} \\ \dot{V} \end{bmatrix} = A_q \begin{bmatrix} v \\ r \\ U \\ V \end{bmatrix} + B_q\delta_f, \tag{11}$$

where

$$M_q = \begin{bmatrix} M_1 & 0_{2\times4} & M_2 \\ M_3 & M_4 & M_5 \\ 0_{2\times2} & M_6 & 0_{2\times2} \end{bmatrix}, \quad A_q = \begin{bmatrix} A_1 & 0_{2\times4} & 0_{2\times2} \\ A_2 & A_3 & A_4 \\ 0_{2\times2} & 0_{2\times4} & A_5 \end{bmatrix},$$

$$B_q = \begin{bmatrix} 2K_f & 2aK_f & 0 & 0 & 2h_fK_f & 0 & 0 & 0 \end{bmatrix}^T,$$

$$M_1 = \begin{bmatrix} m & 0 \\ 0 & I_Z \end{bmatrix}, \quad M_2 = \begin{bmatrix} -h_f m_{sf} & -h_r m_{sr} \\ 0 & 0 \end{bmatrix},$$

$$A_4 = \begin{bmatrix} l_f & 0 \\ 0 & l_r \\ l_f & 0 \\ 0 & l_r \end{bmatrix}, \quad A_5 = \begin{bmatrix} 1 & 0 \\ 0 & 1 \end{bmatrix}.$$

Setting the state vector as $x = \begin{bmatrix} \dot{v} & \dot{r} & \dot{U} & \dot{V} \end{bmatrix}^T$. Then Eq. (11) can be rewritten into Eq. (12):

$$\dot{x} = Ax + B\delta_f, \tag{12}$$

where $A = M_q^{-1} \times A_q, B = M_q^{-1} \times B_q$.

2.3 Determination of the Equivalent Wheelbase

According to Refs. [25, 26], the method to determine the equivalent wheelbase is obtained. First, the linear two-DOF model of the vehicle can be set up based on Eqs. (1) and (2),

$$\begin{cases} \begin{bmatrix} \dot{\beta} \\ \dot{r} \end{bmatrix} = \begin{bmatrix} \frac{-K_f-K_m-K_r}{mu} & \frac{-aK_f+bK_m+cK_r}{mu^2} - 1 \\ \frac{-aK_f+bK_m+cK_r}{I_Z} & \frac{-a^2K_f-b^2K_m-c^2K_r}{I_Z u} \end{bmatrix} \begin{bmatrix} \beta \\ r \end{bmatrix} \\ \qquad + \begin{bmatrix} \frac{K_f}{mu} \\ \frac{aK_f}{I_Z} \end{bmatrix} [\delta_f], \\ \beta = \frac{v}{u}, \end{cases} \tag{13}$$

where β represents side slip angle of mass center.

At steady state, $\dot{\beta} = 0$ and $\dot{r} = 0$, so

$$\begin{bmatrix} \beta \\ r \end{bmatrix} = \begin{bmatrix} \frac{-K_f - K_m - K_r}{mu} & \frac{-aK_f + bK_m + cK_r}{mu^2} - 1 \\ \frac{-aK_f + bK_m + cK_r}{I_Z} & \frac{-a^2K_f - b^2K_m - c^2K_r}{I_Z u} \end{bmatrix}^{-1} \times \begin{bmatrix} \frac{K_f}{mu} \\ \frac{aK_f}{I_Z} \end{bmatrix} [\delta_f]. \tag{14}$$

When only taking the front axle steering into account, the yaw rate gain can be described as follows:

$$\begin{aligned} \frac{r}{\delta_f} = u[K_f K_m(a+b) - K_f K_r(a+c)] \Big/ \{ & K_f K_m (a+b)^2 \\ & + K_f K_r (a+c)^2 + K_m K_r (c-b)^2 \\ & - mu^2 (aK_f - bK_m - cK_r)\}. \end{aligned} \tag{15}$$

Setting

$$\begin{cases} l = a + c, \\ t = c - b. \end{cases} \tag{16}$$

The yaw rate gain can be simplified.

$$\begin{aligned} \frac{r}{\delta_f} = u \Big/ \Big\{ & \left[K_f K_m (l-t)^2 + K_f K_r l^2 + K_m K_r t^2 \right] / \\ & [K_f K_m (l-t) + K_f K_r l] + u^2 [-m(aK_f - bK_m - cK_r)] / \\ & [K_f K_m (l-t) + K_f K_r l] \Big\}. \end{aligned} \tag{17}$$

So, the equivalent wheelbase of the triaxle bus can be obtained according to the equivalence of physical meaning as follows:

$$l_e = \frac{K_f K_m (l-t)^2 + K_f K_r l^2 + K_m K_r t^2}{K_f K_m (l-t) + K_f K_r l}. \tag{18}$$

Then, the equivalent front sprung mass is

$$m_{sf} = \frac{m_s (l_e - a)}{l_e} \tag{19}$$

and the equivalent rear sprung mass is

$$m_{sr} = \frac{m_s a}{l_e}. \tag{20}$$

Also, the equivalent front and rear unsprung mass can be described as

$$\begin{cases} m_{uf} = \dfrac{m_u (l_e - a)}{l_e}, \\ m_{ur} = \dfrac{m_s a}{l_e}. \end{cases} \tag{21}$$

2.4 Parameter Estimation

The torsion stiffness coefficient k_b is an important parameter of the vehicle model, which can be estimated based on steady-state value obtained from the simulation.

According to the above-mentioned roll motions of sprung mass (3), the torsion stiffness coefficient k_b can be represented as follows:

$$\begin{aligned} k_b = \{ & [m_{sf} h_f a_y + m_{sf} g h_f \varphi_{sf} - k_f (\varphi_{sf} - \varphi_{uf}) \\ & - l_f (\dot{\varphi}_{sf} - \dot{\varphi}_{uf}) - I_{xf} \ddot{\varphi}_{sf} - l_b (\dot{\varphi}_{sf} - \dot{\varphi}_{sr})] \} / \\ & (\varphi_{sf} - \varphi_{sr}). \end{aligned} \tag{22}$$

In a steady state response of the vehicle motion equation, the roll velocity and the roll acceleration of the sprung mass and unsprung mass are set to be zero. That is

$$\begin{cases} \dot{\varphi}_{sf} = 0, \\ \dot{\varphi}_{uf} = 0, \\ \dot{\varphi}_{sr} = 0, \\ \ddot{\varphi}_{sf} = 0. \end{cases} \tag{23}$$

The φ_{sf}, φ_{sr}, φ_{uf}, a_y can be obtained from TruckSim. Substituting these into Eq. (22):

$$k_b = \frac{m_{sf} h_f a_y + m_{sf} g h_f \varphi_{sf} - k_f (\varphi_{sf} - \varphi_{uf})}{\varphi_{sf} - \varphi_{sr}}. \tag{24}$$

To demonstrate the accuracy of the above estimations, the torsion stiffness coefficient k_b is calculated according to Eq. (4) in the same method. That is, the torsion stiffness coefficient also can be obtained as follows:

$$k_b = \frac{m_{sr} h_r a_y + m_{sr} g h_r \varphi_{sr} - k_r (\varphi_{sr} - \varphi_{ur})}{\varphi_{sf} - \varphi_{sr}}. \tag{25}$$

From Eq. (24), the torsion stiffness coefficient can be estimated to 3967329 N·m/rad, which is close to the value calculated from Eq. (25). The error is less than 2%.

2.5 Validation of Vehicle Model

To verify the vehicle model, the dynamic performances of a three-axle bus rollover are simulated in TruckSim. A "tour bus 3A" model is used. The three-axle bus runs with the initial vehicle speed of 60 km/h, the front wheel steering angle at 6° in J-turn condition. The triaxle bus parameters are showed in Table 1.

Figure 3 shows the dynamic performances of the triaxle bus rollover. The solid lines are the results simulated by TruckSim model, and the dotted lines are calculated by the theoretical model.

As shown in Figure 3, the simulation and theoretical results are highly consistent with each other. In

Table 1 Parameters of a triaxle bus

Symbol	Value	Unit	Symbol	Value	Unit
K_f	62952	N/rad	h_r	0.575	m
K_m	114829	N/rad	h_{uf}	0.51	m
K_r	62952	N/rad	h_{ur}	0.51	m
I_{xf}	1033.1	kg·m^2	k_f	888433	N·m/rad
I_{xr}	1277.4	kg·m^2	k_r	58843	N·m/rad
I_Z	34693.7	kg·m^2	k_{uf}	489978	N·m/rad
T_{wf}	2.03	m	k_{uf}	489978	N·m/rad
T_{wr}	1.863	m	l_f	3444	N·m·s/rad
a	3.5	m	l_r	3444	N·m·s/rad
b	2.29	m	m	8715	kg
c	3.47	m	m_{sf}	3203	kg
h_{cf}	0.675	m	m_{sr}	3797	kg
h_{cr}	0.675	m	m_{uf}	570	kg
h_f	0.575	m	m_{ur}	1145	kg

Figure 3(a), the peak value of lateral acceleration is 0.4613g simulated by the TruckSim model, and 0.4525g calculated by the theoretical model. Thus, the error of the peak value of lateral acceleration is 1.9%. Also, the steady state value and the reaction time of lateral acceleration can be compared, with errors of 3.8% and 2.2%, respectively.

Similarly, the error of the peak value, the steady state value and the reaction time of yaw rate can be obtained as 4.8%, 2% and 3.1% in Figure 3(b). The error of the peak value, the steady state value and the reaction time of roll angle of front sprung mass can be obtained as 3.4%, 2.3% and 5.5% in Figure 3(c). In addition, the error of the peak value, the steady state value and the reaction time of roll angle of rear sprung mass can be obtained as 2.7%, 2.9% and 5.7% in Figure 3(d).

From the above comparison, the error of vehicle dynamic characteristics between the theoretical model and the TruckSim model are less than 6%. As a result, the accuracy

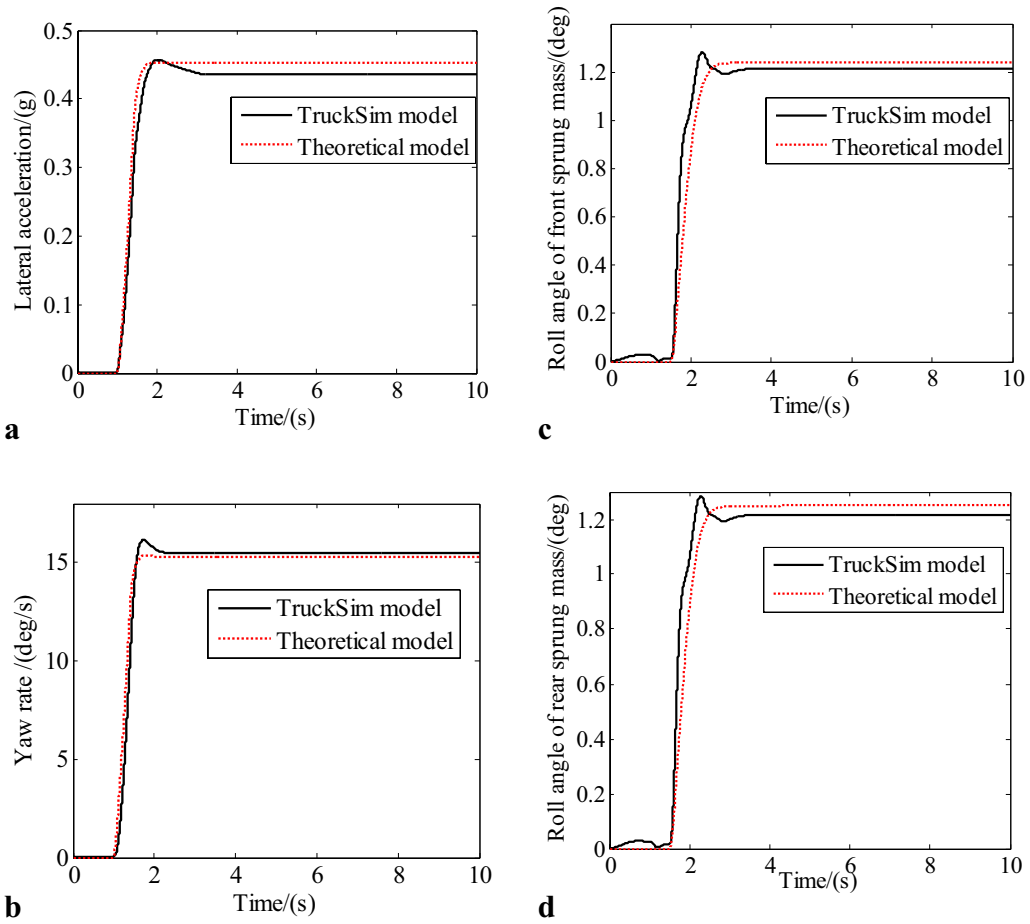

Figure 3 Dynamic performances of a three-axle bus rollover: (**a**) Lateral acceleration, (**b**) Yaw rate, (**c**) Roll angle of front sprung mass, (**d**) Roll angle of rear sprung mass

of the parameter estimation and the validity of the model has been verified.

3 Rollover Index of the Triaxle Bus

To prevent rollover of the triaxle, a precise and real-time rollover index is very necessary. The existing studies on the vehicle rollover mainly focused on the static stability factor (SSF). This measure of rollover propensity only reflects the most fundamental relation in a static condition and does not take the suspension and tire into account [27]. To detect rollover in the process of vehicle movement, the lateral-load transfer ratio (*LTR*) was commonly used by researchers [4–7].

The *LTR* was described as follows:

$$LTR = \frac{F_{\mathrm{L}} - F_{\mathrm{R}}}{F_{\mathrm{L}} + F_{\mathrm{R}}}, \tag{26}$$

where, F_L and F_{R} are the vertical force of the left and right wheels. When the absolute value of *LTR* is equal to 1, the car is considered to roll over [28].

3.1 Establishment of Rollover Index

For the triaxle bus, because of its long wheelbase, the vertical load of the right and left wheels cannot be directly used to judge the rollover. Therefore, it is important to propose a rollover index for both the front and rear. According to the definition, the rollover index can be expressed as follows:

$$\begin{cases} RI_{\mathrm{f}} = \dfrac{F_{L1} - F_{R1}}{F_{L1} + F_{R1}}, \\ RI_{\mathrm{r}} = \dfrac{F_{L2} + F_{L3} - (F_{R2} + F_{R3})}{F_{L2} + F_{L3} + F_{R2} + F_{R3}}, \end{cases} \tag{27}$$

where RI_{f} is the rollover index of front sprung mass system and RI_{r} is the rollover index of rear sprung mass system.

Because the vertical forces of the wheels cannot be measured directly, the rollover index needs to be reformulated according to the developed vehicle model. The vertical acceleration of the tire is ignored. Then Eq. (28) is obtained:

$$\begin{cases} F_{L1} - F_{R1} = F_2 - F_1, \\ F_{L1} + F_{R1} = m_{\mathrm{f}} g, \end{cases} \tag{28}$$

where F_1 and F_2 are the left and right suspension force. According to moment equilibrium equations, the difference value between F_1 and F_2 can be obtained.

$$\frac{T_{\mathrm{wf}}}{2}(F_2 - F_1) = -k_{\mathrm{f}}(\varphi_{\mathrm{sf}} - \varphi_{\mathrm{uf}}) - l_{\mathrm{f}}(\dot{\varphi}_{\mathrm{sf}} - \dot{\varphi}_{\mathrm{uf}}). \tag{29}$$

Combining Eq. (3),

$$F_2 - F_1 = \frac{2}{T_{\mathrm{wf}}}\Big[I_{\mathrm{Xf}}\ddot{\varphi}_{\mathrm{sf}} - m_{\mathrm{sf}}h_{\mathrm{f}}a_{\mathrm{y}} - m_{\mathrm{sf}}gh_{\mathrm{f}}\varphi_{\mathrm{sf}} + k_{\mathrm{b}}(\varphi_{\mathrm{sf}} - \varphi_{\mathrm{sr}})\Big]. \tag{30}$$

Thus,

$$RI_{\mathrm{f}} = -\frac{2}{T_{\mathrm{wf}}}\Big[I_{\mathrm{Xf}}\ddot{\varphi}_{\mathrm{sf}} - m_{\mathrm{sf}}h_{\mathrm{f}}a_{\mathrm{y}} - m_{\mathrm{sf}}h_{\mathrm{f}}g\varphi_{\mathrm{sf}} + k_{\mathrm{b}}(\varphi_{\mathrm{sr}} - \varphi_{\mathrm{sf}})\Big]/m_{\mathrm{f}}g. \tag{31}$$

The RI_{r} can be obtained in the same way,

$$RI_{\mathrm{r}} = -\frac{2}{T_{\mathrm{wr}}}\Big[I_{\mathrm{Xr}}\ddot{\varphi}_{\mathrm{sr}} - m_{\mathrm{sr}}h_{\mathrm{r}}a_{\mathrm{y}} - m_{\mathrm{sr}}h_{\mathrm{r}}g\varphi_{\mathrm{sr}} - k_{\mathrm{b}}(\varphi_{\mathrm{sr}} - \varphi_{\mathrm{sf}})\Big]/m_{\mathrm{r}}g, \tag{32}$$

where T_{wf} and T_{wr} are the front wheel track and the rear wheel track.

RI_{f} and RI_{r} are not identical such that it is necessary to use the larger rollover index to indicate the rollover stability of the vehicle. A new rollover index of the triaxle bus is defined as

$$RI_{\mathrm{t}} = \max[|RI_{\mathrm{f}}|, |RI_{\mathrm{r}}|]. \tag{33}$$

Basically, the triaxle bus is stable when the value of RI_{t} is less than 1, and it is likely to rollover when the value of RI_{t} is over than or equal to 1.

3.2 Validation of Rollover Index

To validate the proposed rollover index, the dynamic performance of the triaxle bus is simulated in TruckSim. The comparison of the *LTR* and RI_{t} in two different cases is obtained in this section.

Case I. J-turn condition is used in this case. The front wheel steering angle is 6°. Therefore, the rollover indices of triaxle bus in J-turn can be obtained.

Figure 4(a) and (b) show comparisons of the rollover index of the front and rear sprung mass when the vehicle speed is 60 km/h. The dotted lines are obtained from the fundamental definition of *LTR*, and the solid lines are the new rollover indices, which are calculated by the above Eqs. (31) and (32). As shown in Figure 4(a), the maximum error between fundamental LTR_{f} and RI_{f} is less than 5%, and the peak value of RI_{f} is a little bigger than *LTR*. That means RI_{f} can be close to the traditional LTR_{f}. In Figure 4(b), a good fit between the LTR_{r} and RI_{r} can be witnessed. In summary, the proposed rollover indices of front sprung mass and the rear sprung mass are efficient.

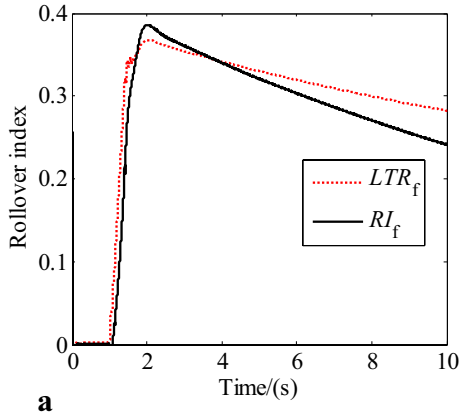

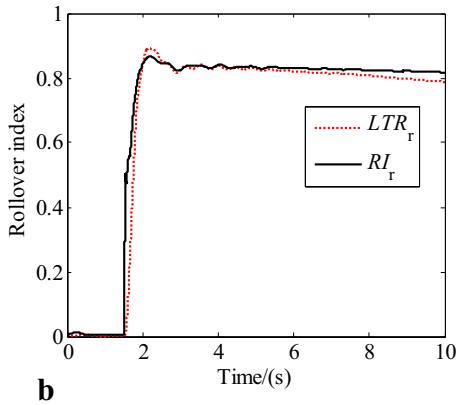

Figure 4 Comparison of new rollover index of front and rear sprung mass and *LTR* in J-turn maneuver: (**a**) Comparison of RI_f and LTR_f in J-turn; (**b**) Comparison of RI_r and LTR_r in J-turn

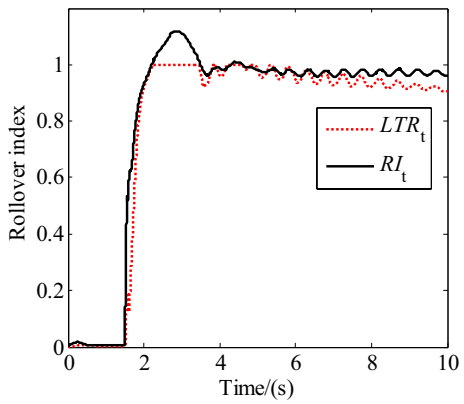

Figure 5 Rollover dynamics of the triaxle bus in J-turn maneuver

To better validate the effectiveness of RI_t, the larger value of *LTR* of front and rear sprung mass is used to compare with RI_t. As shown in Eq. (34):

$$LTR_t = \max(|LTR_f|, |LTR_r|). \tag{34}$$

Figure 5 shows the roll stability of the triaxle bus when the vehicle speed is 90 km/h. The absolute value of both LTR_t and RI_t reach 1 at 2.1 s, and less than 1 a 3.5 s. That is, one side of the wheels lift off the ground from 2.1 s to 3.5 s. This further proves the accuracy of RI_t.

Case II. In this case, another standard rollover test condition is implemented, Fishhook, with the amplitude of the front wheel steering angle set to 6°.

As shown in Figure 6, when the vehicle speed is 60 km/h, the theoretical rollover index of front sprung mass system and rear sprung mass make an agreement with the LTR_f and the LTR_r simulated by TruckSim. It demonstrates the validation of the proposed index in Fishhook condition.

Figure 7 shows the roll dynamics of the triaxle bus in the Fishhook condition when the vehicle operates at 90 km/h. The RI_t also agrees with the LTR_t simulated by TruckSim. In addition, the value of the new rollover index and the LTR_t reach 1 at the same time such that the RI_t can also predict rollover risk of the triaxle bus in the Fishhook condition.

4 Roll Stability of the Triaxle Bus

4.1 Roll Stability in Typical Maneuvers

To study the dynamic rollover stability of the triaxle bus, this section presents three typical rollover maneuvers, which include the J-turn maneuver, the Fishhook maneuver, and the Double-lane-change maneuver. The parameters of the triaxle bus are shown in Table 1.

J-turn maneuver. In this maneuver, the road adhesion coefficient is 0.85, and the front wheel steering angle is 6°.

As shown in Figure 8, the solid line, dashed line, and dotted line represent the roll dynamic response of the triaxle bus when the vehicle moves at 60 km/h, 80 km/h and 100 km/h, respectively. When the speed reaches 100 km/h, the value of the rollover index of the vehicle is over 1 at 2.1 s, and the vehicle is at risk of rollover. When the vehicle moves slowly, the value of RI_t is also decreased. Therefore, when the steering angle input is a constant, with the higher speed, the vehicle is more likely to rollover.

Fishhook maneuver. This is a severe rollover test condition. The amplitude of the front wheel steering angle is set to 4°, the road adhesion coefficient is 0.85.

In Figure 9, the triaxle bus will not be at risk of rollover at 60 km/h, 80 km/h and 100 km/h in the first phase of the Fishhook condition (before 3.5 s). In the second phase of the Fishhook condition, the bus rolls over at less than four seconds, with a speed of 100 km/h. Like the J-turn condition, the value of RI_t decreases with the decrease of vehicle speed. Compared with the results

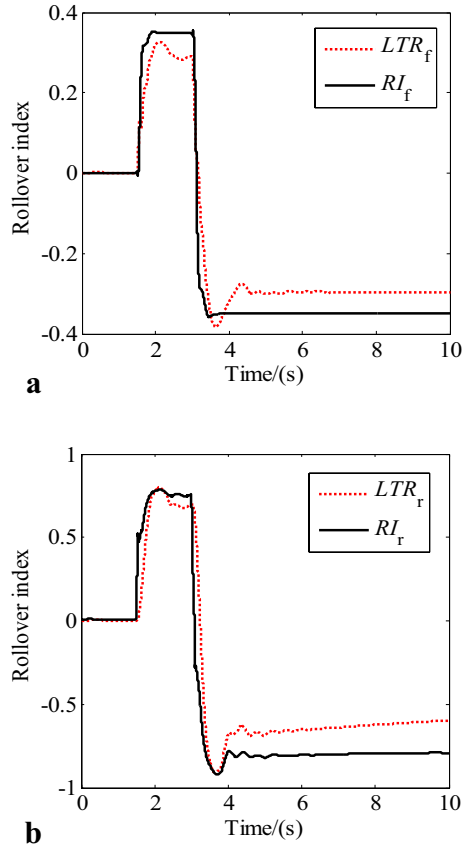

Figure 6 Comparison of new rollover index of front and rear sprung mass and LTR in Fishhook maneuver: (**a**) Comparison of RI_f and LTR_f in Fishhook; (**b**) Comparison of RI_r and LTR_r in Fishhook

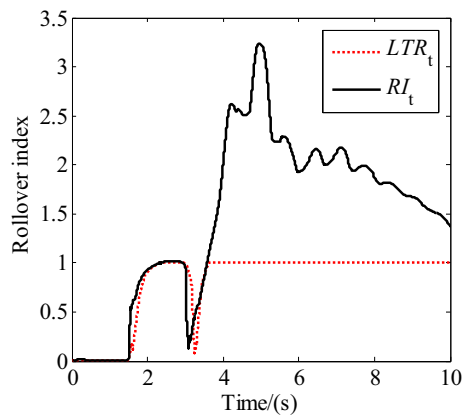

Figure 7 Rollover dynamics of the triaxle bus in Fishhook maneuver

of J-turn condition, the rollover happens easier in the Fishhook condition.

Double lane change (DLC) maneuver. The rollover stability in a DLC condition is also studied. The road adhesion coefficient is 0.85, and its width is 3.5 m. The movement track of triaxle bus in DLC condition is shown in Figure 10.

In DLC condition, although the value of RI_t at 100 km/h is larger than the value of RI_t at 80 km/h and 60 km/h, it will not roll over. Therefore, the triaxle bus has good roll stability in the DLC condition. Similar to the J-turn and Fishhook conditions, the value of RI_t decreases with the decrease of vehicle speed, that is, reducing the vehicle speed is an effective measure to decrease the risk of the triaxle bus rollover in typical maneuvers.

In conclusion, the fishhook condition is the most dangerous. In the actual driving process, the driver should avoid repeatedly pounding the steering wheel. Furthermore, it is observed that the higher the vehicle speed, the worse the stability.

4.2 Factors of Vehicle Structure

To analyze the effect law of some key vehicle structure parameters on the roll stability, Figure 11 presents the stability regions with respect to the vehicle critical speed and a changeable vehicle structure parameter when other vehicle parameters are fixed as constants. The vehicle is asymptotically stable for the vehicle speed u, is less than the rollover critical speed u_c, and unstable for $u > u_c$.

As shown in Figure 11(a), the farther the distance between the second axle and the third axle, the smaller the stability region is. Thus, the shorter distance between them can be used to reduce rollover accidents in the future.

The sprung mass of vehicle will be heavier as the number of passengers increase. Figure 11(b) illustrates the impact of ratio of the rear sprung mass to the unsprung mass on rollover stability. Given 25 passengers, 60 kg per person and 7.5 kg of luggage per person in the rear space of triaxle bus, the ratio will increase about 0.9 when the triaxle bus is fully loaded and the critical speed will decrease about 9 km/h. Thus, when designing the triaxle bus, the sprung mass of the empty bus should be small enough to improve the rollover stability.

The roll axle is usually with a certain angle to the ground, the value of this angle also affects the roll performance. Figure 11(c) shows the impact of the angle between the roll axle and horizontal plane on rollover stability. It can be found that the rollover stability improves when the roll axle is low in the rear axle and high in the front axle.

The effects of torsion stiffness should be discussed to reflect the effect of roll coupling of each axle on rollover. As shown in Figure 11(d), larger torsion stiffness

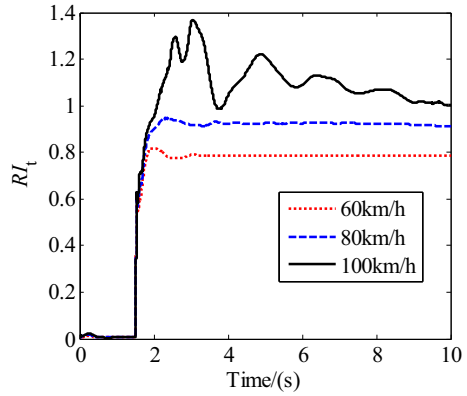

Figure 8 RI_t in J-turn maneuver

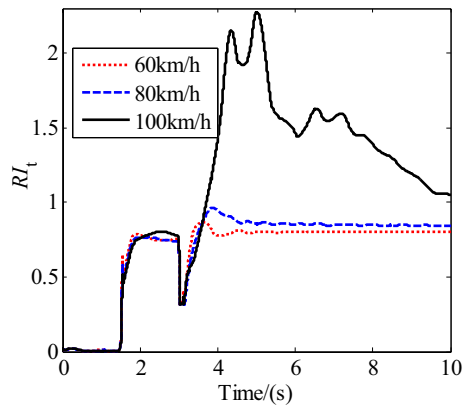

Figure 9 *RI*t in Fishhook maneuver

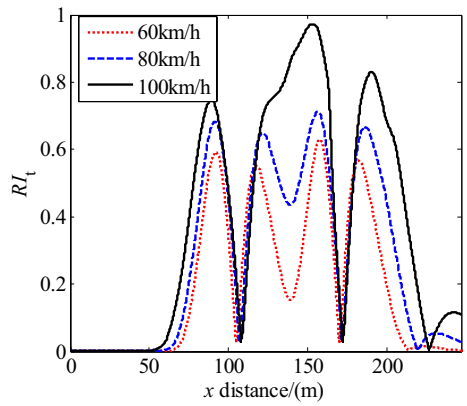

Figure 10 RI_t in Double Lane Change maneuver

can reduce the difference between front rollover system and rear rollover system, thus enhance the rollover stability of triaxle bus.

In addition, this paper also does research on the rollover index under parameter uncertainties, especially tire parameters. Because equivalent sprung masses and equivalent wheel base is a function of cornering stiffness. These tire parameters can change as vertical tire forces vary. The vertical tire forces can change dramatically since the scenario dealt with in this paper is related to rollover and the mass of the bus can vary with a wide range depending on the number of passengers. So the impact of the cornering stiffness of tires on rollover stability is analyzed in Figure 12.

As shown in Figure 12(a), when the K_f increase, the rollover stability becomes worse. Because larger K_f can increase the yaw moment; To the contrary, the middle and rear wheels are located behind the center of mass. When the corning stiffness increases, the yaw moment decreases, thus the rollover stability is improved, as shown in Figure 12(b) and (c).

4.3 Factors of Vehicle Driving

The study of driving parameters is helpful to make suggestions on the driver's operation. This section will analyze the influence of the driving parameters including the steering angle and road adhesion coefficient on rollover stability.

As shown in Figure 13(a), with the increase of steering angle, the maximum value of RI_t is increased linearly, showing the critical value of steering angle is 6.8° when the vehicle speed is 60 km/h. Furthermore, the largest front wheel steering angle only changes 2.4°, but the RI_t increases from 0.7 to 1. Therefore, reducing the largest front wheel steering angle has an obvious effect on improving the rollover stability.

Figure 13(b) represents the maximum value of RI_t at various road adhesion coefficients. It shows that the maximum value of RI_t grows almost linearly from 0.5 to 1.08 as the road adhesion coefficient increases before 0.625. When the road adhesion coefficient is too low, the generated lateral force is not enough to support the steering of the vehicle, resulting in less roll movement. When the road adhesion coefficient changes from 0.625 to 1.2, RI_t exhibits a negative correlation with the road adhesion coefficient. Thus, when the road adhesion efficient is near 0.6, the rollover stability is poor.

5 Rollover Stability under External Disturbances

The triaxle bus encounters various interferences during driving, such as lateral force interference and vertical interference. Interference factors may lead the triaxle bus to roll over around the tipping point. Therefore, it is very important to understand the influence of interference factors on the rollover stability of the triaxle bus. The

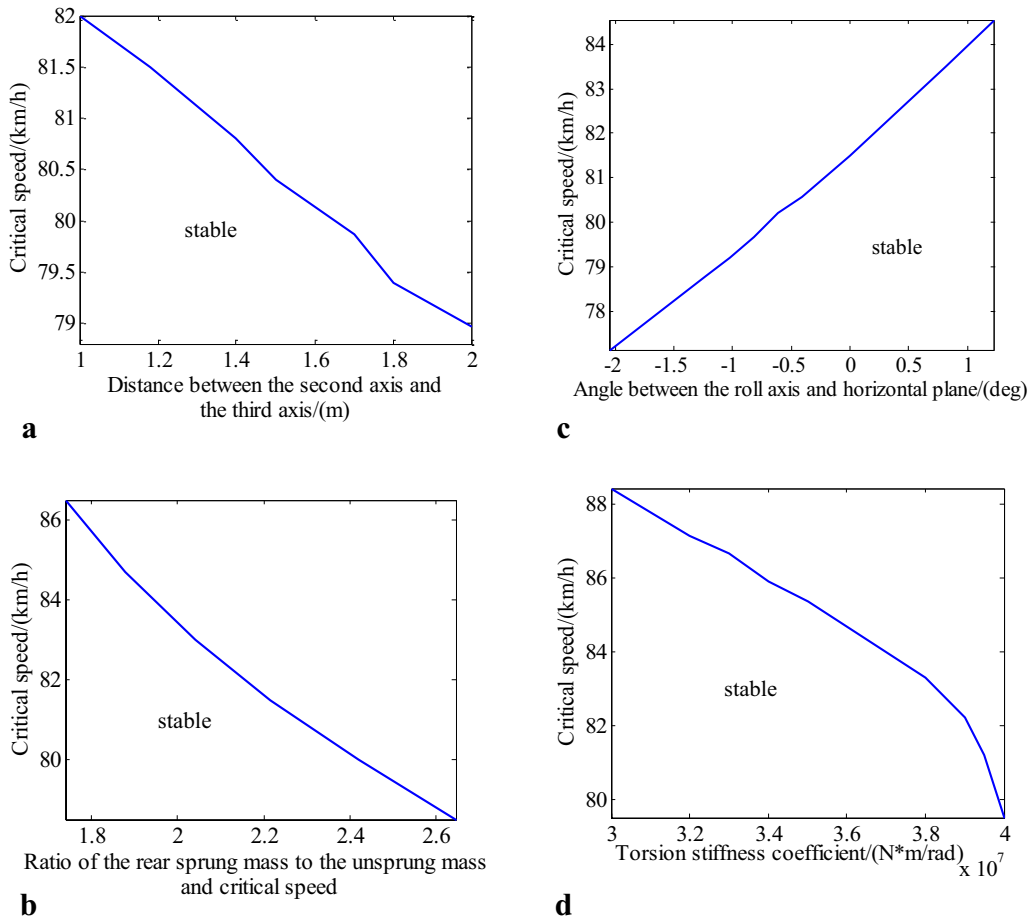

Figure 11 Impact of various structure parameters on rollover stability: (**a**) Impact of distance between the second axle and the third axle; (**b**) Impact of ratio of the rear sprung mass to the unsprung mass; (**c**) Impact of angle between the roll axle and horizontal plane; (**d**) Impact of various torsion stiffness of vehicle body

J-turn maneuver is selected to simulate rollover stability with external disturbance.

5.1 External Vertical Force

When the triaxle bus moves at 80 km/h, a pulse signal of vertical force is applied to a wheel from 2.0 s to 2.2 s. Figure 14(a) shows the maximum values of RI_t when the external vertical force is applied to the inside wheel on different axles. The amplitude of the external vertical force on the front axle has little influence on vehicle rollover stability. If the vertical force is applied to the wheel of the second axle, the maximum value of RI_t increases when the amplitude of the external vertical force increases. When it increases to 2700 N, the triaxle bus has rollover risk. The maximum value of RI_t increases when the external vertical force on the third axle is less than 2300 N. It shows the external vertical force applied to the inside wheel will deteriorate the rollover stability, and when the disturbance is applied to the inside wheel on the third axle, the vehicle is much easier to rollover risk than when it is applied to the inside wheel on other axles.

Figure 14(b) shows the maximum values of RI_t when the vertical force disturbs the outside wheel on different axles. With the increasing amplitude of the vertical force applied to the wheel on the second axle and the third axle, the RI_t increases, meaning the rollover stability becomes worse. It also can be found that the vehicle is more likely to roll over when it is applied to the inside wheel on the third axle than when it is applied to the inside wheel on other axles. On the contrary, the larger amplitude of the vertical force applied to the wheel on the front axle, the vehicle will be more stable. Therefore, the vertical force applied to the outside wheel on the front axle can offset the rollover tendency.

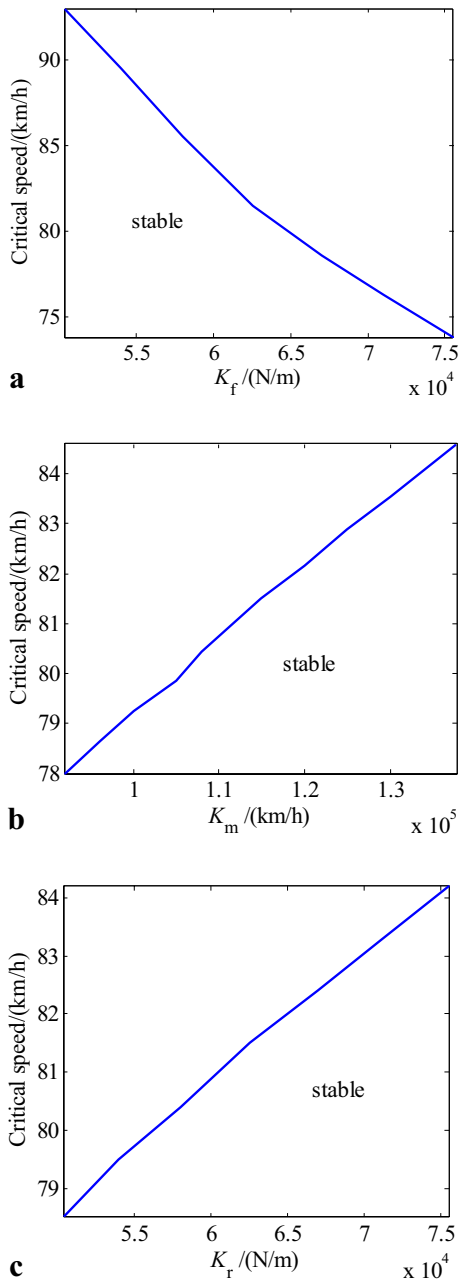

Figure 12 Impact of the cornering stiffness of tires on rollover stability: (**a**) K_f; (**b**) K_m; (**c**) K_r

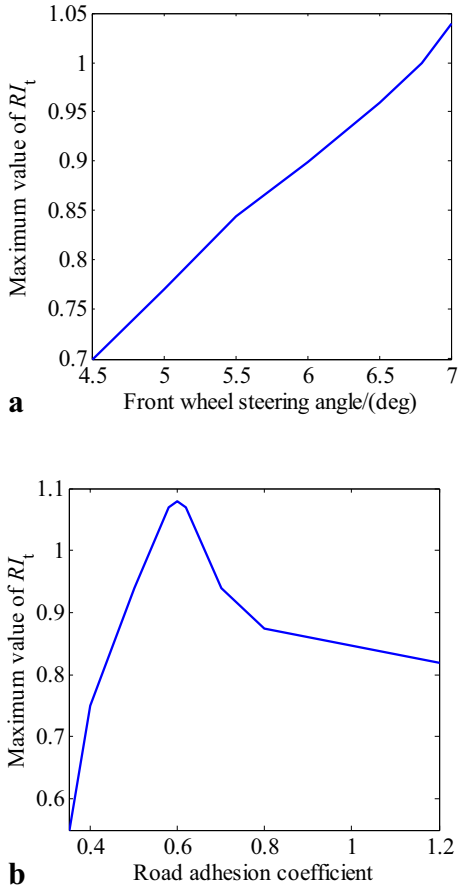

Figure 13 Impact of different driving parameters on rollover stability. (**a**) Impact of front wheel steering angle; (**b**) Impact of road adhesion coefficient

Figure 15 shows the phase plane trajectory of the triaxle bus with the 6000 N vertical force on the outside wheel of the third axle. The trajectory shows that the vehicle is stable when the bus is not disturbed but the vehicle will roll over with the disturbance applied to the outside wheel on the third axle. It intuitively reflects that the vertical force applied to the wheels can affect the rollover stability.

5.2 External Lateral Force

When the triaxle bus moves at 80 km/h, a pulse signal of lateral force is applied to a wheel from 2.0 s to 2.2 s. Figure 16(a) shows the maximum values of RI_t when the lateral force interference is applied to the inside wheels on different axles. When the front axle is disturbed, the yaw rate of the triaxle bus will increase, causing over-steering and rollover. In Figure 16(a), the maximum value of RI_t increases with the amplitude of the lateral force increasing. When the amplitude of the lateral force on the wheel of the second axle is less than 1800 N, or the amplitude of the lateral force on the wheel of the third axle is less than 2600 N, the greater the amplitude of the interference, the smaller the maximum value of RI_t. Because the second axle and the third axle are located behind the center of gravity of the triaxle bus, the lateral interference

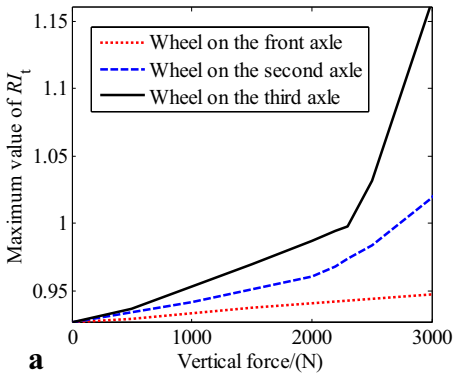

Figure 14 Influence of vertical interference on rollover stability of the triaxle bus: (**a**) RI_t with vertical force interference applied to the inside wheel; (**b**) RI_t with vertical force interference applied to the outside wheel

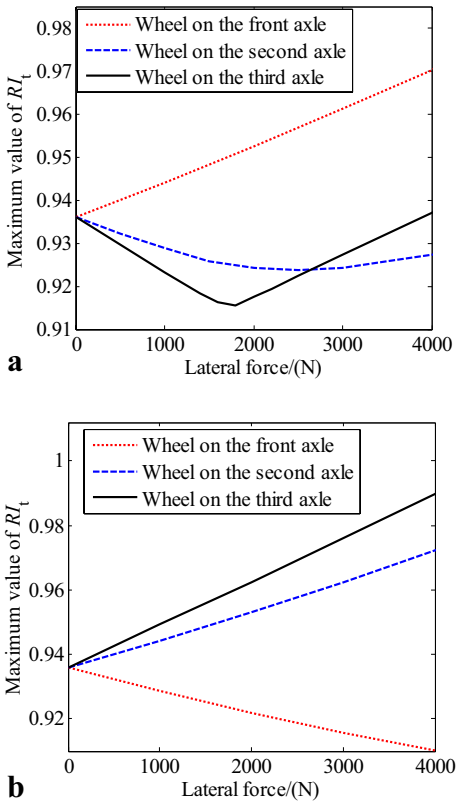

Figure 16 Influence of lateral interference on absolute maximum value of RI_t without controlling: (**a**) RI_t with lateral force interference applied to the inside wheel; (**b**) RI_t with lateral force interference applied to the outside wheel

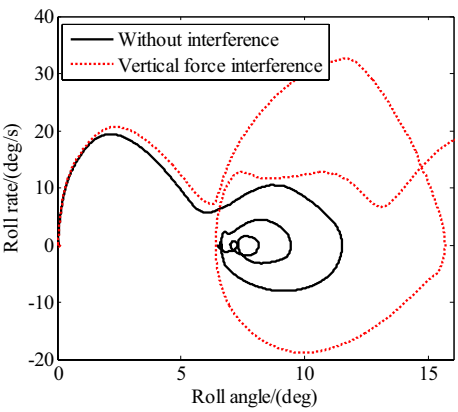

Figure 15 Diagram of $(\varphi - \dot{\varphi})$ with vertical force interference

will resist steering and then reduce the yaw rate of the triaxle bus. Thus, the rollover stability improves. If the lateral interference on the wheel of the second axle and the third axle continues to increase, the torque of lateral interference to the center of sprung mass is large enough to increase the rollover risk of the triaxle bus. Thus, the maximum value of RI_t increases. In addition, the distance between the third axle and the center of gravity is further than that between the second axle and the center of gravity, therefore, the lateral interference to the third axle is more sensitive.

Contrary to Figure 16(a), when the second axle and the third axle are disturbed by the lateral force applied to the outside wheel, the yaw rate of the triaxle bus will increase and the triaxle bus has rollover risk. However, the lateral force on the front axle can reduce the oversteering to avoid the occurrence of rollover, as shown in Figure 16(b).

Figure 17 shows the phase plane trajectory of the triaxle bus subjected to 5000 N of the lateral force interference. When the triaxle bus is disturbed by the excessive lateral force on the outside wheel on the third axle, the roll angle and roll rate varies greatly.

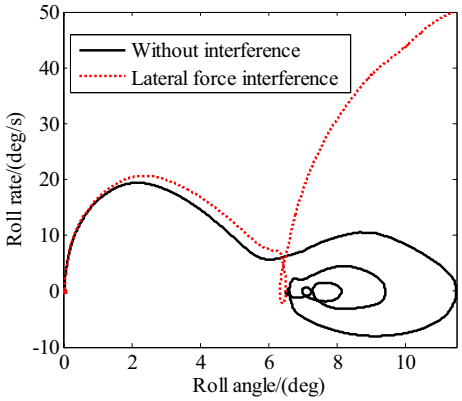

Figure 17 Diagram of with ($\varphi - \dot{\varphi}$) lateral force interference

6 Conclusions

(1) Taking the effect of torsion deformation of vehicle body into consideration, a new 6-DOF vehicle model was derived by dividing the triaxle bus into two parts, the second and third axle are equivalent to a virtual rear axle.

(2) The equivalent distance from the center of gravity to the rear virtual axle is derived using the wheelbases of the second axle and the third axle. Furthermore, the torsion stiffness of the vehicle body is estimated.

(3) A new rollover index was proposed to evaluate the rollover risk of the triaxle bus, and evaluated in some numerical cases, the results show that the proposed index has a good ability to detect rollover.

(4) The stability analysis showed that the distance between the second axle and the third axle and the torsion stiffness of vehicle body have great influence on the rollover stability of the triaxle bus, and it is more prone to rollover when the lateral force interference applied to the wheel on the third axle.

Authors' Contributions
ZJ was in charge of the whole trial; JL and AK wrote the manuscript; YH assisted with sampling and laboratory analyses. All authors read and approved the final manuscript.

Acknowledgements
The authors sincerely thanks to Mr. Chao Wang of *Nanjing University of Aeronautics and Astronautics* for his critical discussion and reading during manuscript preparation.

Authors' Information
Zhilin Jin, born in 1978, is currently an associate professor at *Department of Vehicle Engineering, Nanjing University of Aeronautics and Astronautics, China.* He received his PhD degree from *Nanjing University of Aeronautics and Astronautics, China*, in 2008. His research interests include vehicle system dynamics and control.

Jingxuan Li, born in 1997, is currently a master candidate at *Department of Vehicle Engineering, Nanjing University of Aeronautics & Astronautics, China.*

Yanjun Huang, born in 1986, is currently an assistant professor at *Department of Mechanical & Mechatronics Engineering, University of Waterloo, Canada.*

Amir Khajepour, born in 1962, is currently a professor at *Department of Mechanical & Mechatronics Engineering, University of Waterloo, Canada.*

Competing Interests
The authors declare no competing financial interests.

Funding
Supported by National Natural Science Foundation of China (Grant No. 51775269).

Author Details
[1] Department of Vehicle Engineering, Nanjing University of Aeronautics & Astronautics, Nanjing, Jiangsu Province 210016, China. [2] Department of Mechanical & Mechatronics Engineering, University of Waterloo, Waterloo, ON N2L 3G1, Canada.

Received: 24 April 2019 Revised: 19 June 2019 Accepted: 8 July 2019
Published online: 23 July 2019

References

[1] National Highway Traffic Safety Administration. *Traffic safety facts 2014: a compilation of motor vehicle crash data from the fatality analysis reporting system and the general estimates system.* US, Department of Transportation, Washington, DC, 2016: 70-77.

[2] H Huang, R Yedavalli, D Guenther. Active roll control for rollover prevention of heavy articulated vehicles with multiple-rollover-index minimization. *Vehicle System Dynamics*, 2012, 50(3): 471-493.

[3] G Yu, H Li, P Wang, et al. Real-time bus rollover prediction algorithm with road bank angle estimation. *Chaos Solitons & Fractals*, 2016, 89(2): 270-283.

[4] G Yu. Road bank estimation for bus rollover prediction. *Applied Mathematics & Information Sciences*, 2013, 7(5): 2027-2034.

[5] Y Zhang, A Khajepour, X Xie. Rollover prevention for sport utility vehicles usi0ng a pulsed active rear-steering strategy. *Proceedings of the Institution of Mechanical Engineers Part D: Journal of Automobile Engineering*, 2016, 230(9): 1239-1253.

[6] Z Jin, L Zhang, J Zhang, et al. Stability and optimized H∞ control of tripped and untripped vehicle rollover. *Vehicle System Dynamics*, 2016, 54(10): 1405-1427.

[7] W Bao, S Hu. Vehicle rollover simulation analysis considering road excitation. *Transactions of the Chinese Society of Agricultural Engineering*, 2015, 31(2): 59-65.

[8] Y Pourasad, M Mahmoodi-K, M Oveisi. Design of an optimal active stabilizer mechanism for enhancing vehicle rolling resistance. *Journal of Central South University*, 2016, 23(5): 1142-1151.

[9] F Yakub, S Lee, Y Mori. Comparative study of MPC and LQC with disturbance rejection control for heavy vehicle rollover prevention in an inclement environment. *Journal of Mechanical Science & Technology*, 2016, 30(8): 3835-3845.

[10] D Tan, H Wang, Q Wang. Study on the rollover characteristic of In-Wheel-Motor-Driven electric vehicles considering road and electromagnetic excitation. *Shock and Vibration*, 2016, 2016(10): 1-13.

[11] J Na, T Wang, C Wu, et al. A four-node membrane element model with bending modification for one-step algorithm for bus rollover impact. *Engineering Computations*, 2015, 32(3): 607-620.

[12] C Bojanowski. Comprehensive rollover testing of paratransit buses. *International Journal of Heavy Vehicle Systems*, 2013, 20(1): 76-98.

[13] W Liu, H He, F Sun, et al. Integrated chassis control for a three-axle electric bus with distributed driving motors and active rear steering system. *Vehicle System Dynamics*, 2017, 55(5): 1-25.

[14] F Li, G Li, C Ran, et al. Speed calculation model and simulation of rollover prevention in condition of extreme turn based on lateral force coefficient. *Transactions of the Chinese Society of Agricultural Engineering*, 2016, 32(3): 41-47.

[15] J Rath, M Defoort, K Veluvolu. Rollover index estimation in the presence of sensor faults, unknown inputs, and uncertainties. *IEEE Transactions on Intelligent Transportation Systems*, 2016, 17(10): 2949-2959.
[16] G Phanomchoeng, R Rajamani. New rollover index for the detection of tripped and untripped rollovers. *IEEE Transactions on Industrial Electronics*, 2013, 60(10): 4726-4736.
[17] H Li, Y Zhao, H Wang, et al. Design of an improved predictive LTR for rollover warning systems. *Journal of the Brazilian Society of Mechanical Sciences & Engineering*, 2017, 39(10): 3779-3791.
[18] Z Jin, J Weng, J Zhang, et al. Dynamic stability of a driver-vehicle rollover system with time delay. *International Journal of Vibration Engineering & Technology*, 2014, 2(1): 59-71.
[19] Y Li, W Sun, J Huang, et al. Effect of vertical and lateral coupling between tyre and road on vehicle rollover. *Vehicle System Dynamics*, 2013, 51(8): 1216-1241.
[20] D Odenthal, T Bunte, J Ackermann. Nonlinear steering and braking control for vehicle rollover avoidance. *Control Conference*, IEEE, 2015: 598-603.
[21] H Imine, M Djemaï. Switched control for reducing impact of vertical forces on road and Heavy-Vehicle rollover avoidance. *IEEE Transactions on Vehicular Technology*, 2015, 65(6): 4044-4052.
[22] P Gaspar, I Szaszi, J Bokor. Brake control to prevent the rollover of heavy vehicles based on a linear parameter varying model. *European Control Conference*, IEEE, 2015: 3100-3105.
[23] V T Vu, O Sename, L Dugard, et al. H∞ active anti-roll bar control to prevent rollover of heavy vehicles: a robustness analysis. *IFAC-Papers Online*, 2016, 49(9): 99-104.
[24] D Wollherr, J Mareczek, M Buss, et al. Rollover avoidance for steerable vehicles by invariance control. *Control Conference*, IEEE, 2015: 3522-3527.
[25] Y Zhang, Y Huang, H Wang, et al. A comparative study of equivalent modelling for multi-axle vehicle. *Vehicle System Dynamics*, 2018, 56(2): 1-18.
[26] D Williams. On the equivalent wheelbase of a three-axle vehicle. *Vehicle System Dynamics*, 2011, 49(9): 1521-1532.
[27] Z Jin, J Weng, H Hu. Rollover stability of a vehicle during critical driving manoeuvres. *Proceedings of the Institution of Mechanical Engineers Part D: Journal of Automobile Engineering*, 2007, 221(9): 1041-1049.
[28] H Imine, A Benallegue, T Madani, et al. Rollover risk prediction of heavy vehicle using High-Order Sliding-Mode observer: Experimental results. *IEEE Transactions on Vehicular Technology*, 2014, 63(6): 2533-2543.